Fluidity as modulated by pharmacological challenges to the cell

In experiments considering pharmacological challenges that perturbed different subcellular networks and structures, we used the following reagents and concentrations: latrunculin (Millipore #428026, up to 5 μM, from 1 mM stock sol'n in DMSO), to bind actin monomers and drive filamentous actin depolymerization; jasplakinolide (Calbiochem #420107, 1 μM, from 1 mM stock sol'n in DMSO), to promote actin polymerization and filament stabilization; nocodazole (Sigma #M1404, up to 30 μM, from 33 mM stock sol'n in DMSO), to bind tubulin monomers and drive microtubule depolymerization; paclitaxel (Enzo #BML-T104, 5 μM, from 5 mM stock sol'n in DMSO), to stabilize microtubules; acrylamide (#161-0140, 5 μM, from 40% stock sol'n in water), to disrupt intermediate filaments; blebbistatin (Sigma #B0560, 50 μM, from 50 mM stock sol'n in DMSO), to bind myosin and inhibit actomyosin contraction; ML-7 (Biomol, 500 μM, from 22 mM stock sol'n in DMSO), to inhibit actomyosin contraction; histamine (Sigma #H7125, 500 μM, from 9 mM stock sol'n in DMSO), to promote actomyosin contraction; staurosporine (Enzo #ALX-380-014, 10 μM, from 1 mM stock sol'n in DMSO), to inhibit protein kinase activity; methyl-β-cyclodextran (MβCD, Sigma Aldrich #C4555, 20 mM) to insert or deplete cholesterol in the membrane; and cholesterol (Sigma Aldrich #C3045, 4 mM).

The following table shows the fluidity (mean and standard deviation) for CH27 cell populations exposed to each of these pharmaceutical challenges. Only in the case of latrunculin did we see an unambiguous coupled change in fluidity and stiffness, as discussed in the text. Note that although initial concentration ranges were taken from literature reports of measurable changes of cells in the attached-cell state (typically via cytoskeletal network staining), most of these reagent concentrations did not induce significant changes in fluidity in the suspended-cell state. Figure S1 demonstrates this even over a range of concentrations for nocodazole. Thus, we focused our studies on the reagent that induced the largest measurable change in fluidity, latrunculin.

TABLE I: (Supplemental) Cell fluidity as modulated by pharmaceutical challenge. Error is standard deviation.

Intended perturbation	Chemical	Maximum Concentration	Data set size (cells)	Fluidity	Notes
Control	None	None	399	0.24 ± 0.09	
Drug vehicle	DMSO	1%	55	0.26 ± 0.10	
Actin	Latrunculin	5 μM	38	0.38 ± 0.10	Dose dependence in Fig. 5 of main text
	Jasplakinolide	1 μM	40	0.31 ± 0.07	
Microtubules	Nocodazole	30 μM	41	0.24 ± 0.14	Dose dependence in Fig. S1
	Paclitaxel	5 μM	55	0.29 ± 0.14	30% of cells had SNR$<$1
Intermed. fil.	Acrylamide	5 mM	75	0.18 ± 0.13	
Actomyosin	Blebbistatin	50 μM	60	0.18 ± 0.07	
	ML-7	30 μM	40	0.25 ± 0.07	
	Histamine	500 μM	40	0.30 ± 0.09	
	Staurosporine	10 μM	40	0.19 ± 0.07	
Membrane	MβCD	20 mM	35	0.17 ± 0.09	Failed membranes on 38% of cells
	MβCD, cholesterol	20 mM	40	0.24 ± 0.09	4mM cholesterol to enrich
Metabolism	ATP depletion cocktail⋆	see [1]	20	0.39 ± 0.02	Control was a = 0.39 at 1 W/fiber
Cell life	Glutaraldehyde⋆	5%	20	0.18 ± 0.08	Control was a = 0.39 at 1 W/fiber

⋆Reprinted from previous report [1] for comparison.

Calculation of the invariant point

As discussed in the main text, coupled changes in fluidity and stiffness can be thought of as the pivoting of a line around an invariant point (ω_{inv}, G_{inv}). The location of this point was estimated by solving for the most likely intersection of multiple lines, with more weight given to lines representing larger data sets of cells. Bootstrapping was used to estimate the uncertainty in this fitted point; our approach is shown graphically in Fig. S1 (a−e, 100 iterations shown for clarity; a′−e′, 10,000 iterations shown to illustrate convergence).

A single line is obtained from each drug concentration in Fig. 5(a,b), including the control condition. Here, each fluidity-stiffness pair of values, obtained by testing n_i cells, is taken to represent (in the log-transformed domain) a line with slope a_i (and therefore normal unit vector $\hat{e}_i = (a_i\hat{\imath} - \hat{\jmath})/(a_i^2 + 1)^{1/2}$) that passes through the point $p = (\ln \omega_0, \ln G'(\omega_0))$ where $\omega_0/2\pi = 5$ Hz for these experiments (Fig. S1(a)). The penalty for missing the common intersection $x = (\ln \omega_{\text{inv}}, \ln G_{\text{inv}})$ is $n_i \|(x - p_i) \cdot \hat{e}_i\|^2$. By minimizing the total penalty with respect to x, we obtain

$$x = \left(\sum_i n_i \hat{e}_i \hat{e}_i' \right)^{-1} \left(\sum_i n_i \hat{e}_i \hat{e}_i' p_i \right).$$

A 95% confidence interval around this estimate was acquired by first bootstrapping at the cell level to obtain a group of intersection point estimates (Fig. S1(b,b′)). We then simplified the shape of the cluster of bootstrapped estimates in the log-transformed domain by subtracting the resulting slope (Fig. S1(c,c′)), and normalizing by standard deviation along both axes (Fig. S1(d,d′)). The result is a near-circular distribution of points that is amenable to identification of the 95% of points closest to the origin (e.g., by the `ConvexHull` command in Mathematica (Wolfram Research)) (Fig. S1(d,d′)). Finally, the shaping was then undone to enable positioning and overlay on the original plot (Fig. S1(e,e′)).

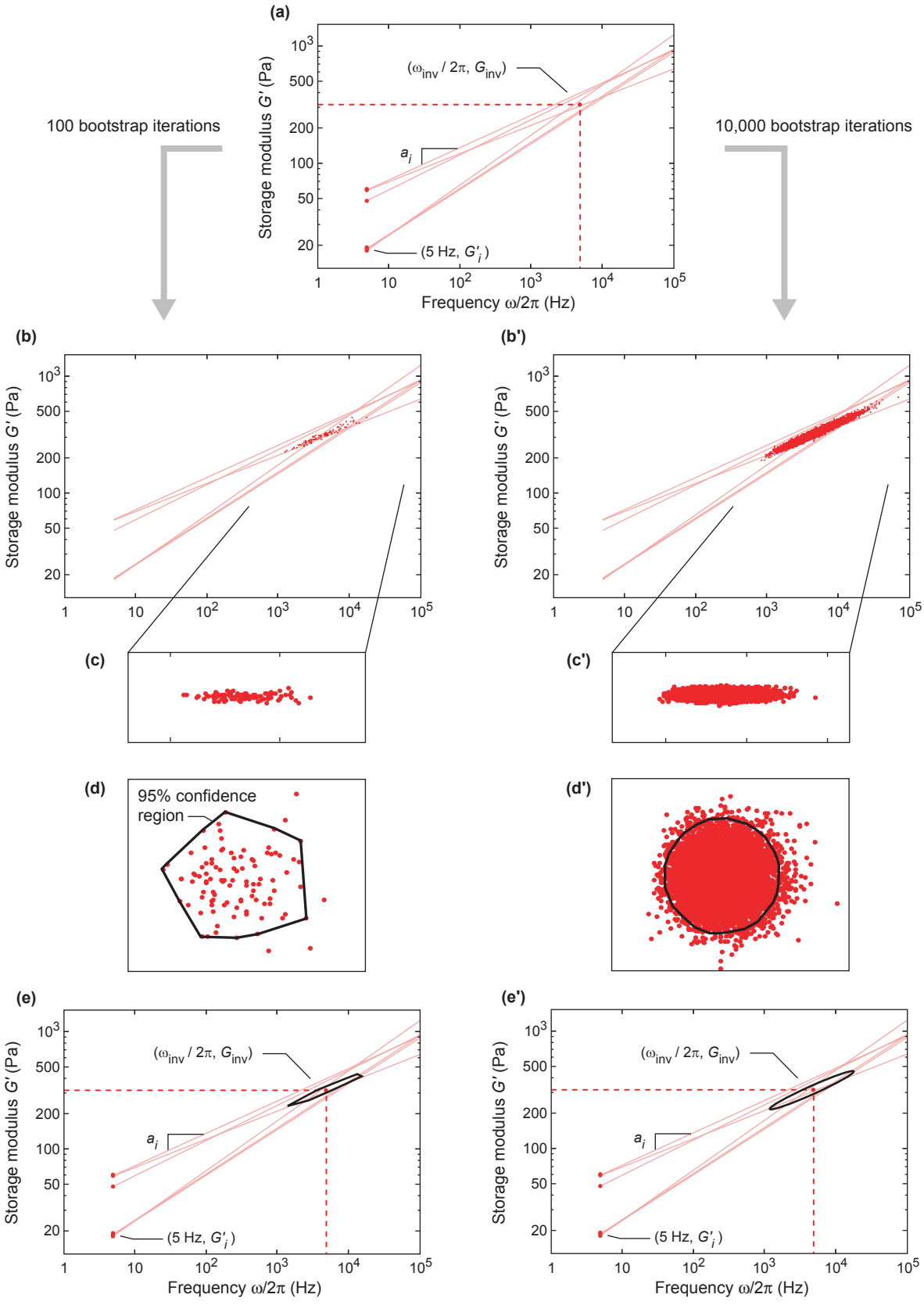

FIG. 1: (Supplemental) Coupled changes in whole-cell fluidity a and stiffness (as storage modulus G') can be visualized as pivoting around an invariant point, the position of which was estimated via least-squares minimization and the uncertainty of which was determined via bootstrapping.

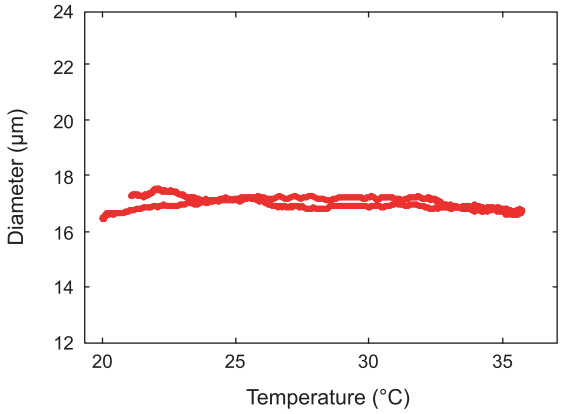

FIG. 2: (Supplemental) A temperature increase from 20°C to 37°C causes no detectable change in CH27 cell size over a timescale of seconds; 100-cell moving average of 639 cells measured while heating and subsequently cooling an optical stretcher chamber augmented with resistive heaters [1]. Each cell was brought into the chamber and allowed to equilibrate for several seconds before size measurement.

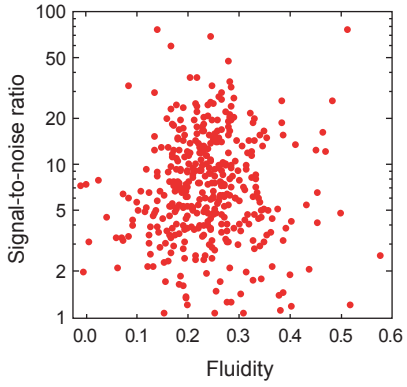

FIG. 3: (Supplemental) Signal-to-noise ratio is uncorrelated with fluidity in CH27 lymphoma cells deformed via oscillatory optical stretching at 0.7 W/fiber mean laser power and 0.5 W/fiber amplitude. Deformation signals acquired using these settings are sufficiently large that fluidity (i.e., phase lag) fitting error is negligible (Fig. 4(c)) compared to intrinsic variation of fluidity in cells, shown by the range of values here.

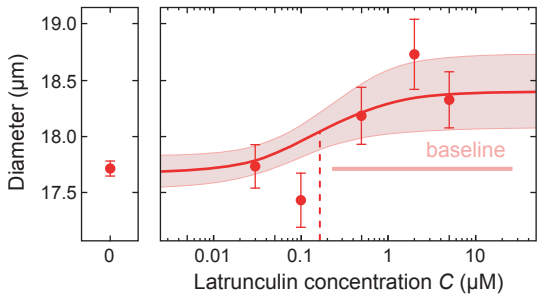

FIG. 4: (Supplemental) Latrunculin causes a detectable and dose-dependent size increase in suspended CH27 cells, from an average diameter of 17.7 μm to 18.4 μm.

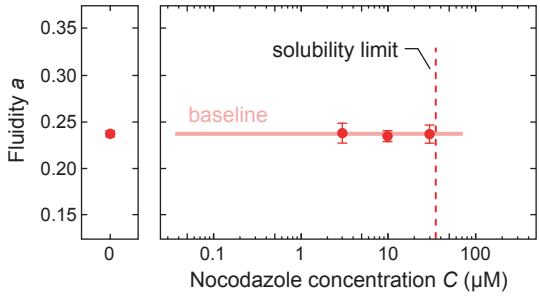

FIG. 5: (Supplemental) Nocodazole does not detectably alter fluidity in suspended CH27 cells, as measured by oscillatory optical stretching, up to the solubility limit.

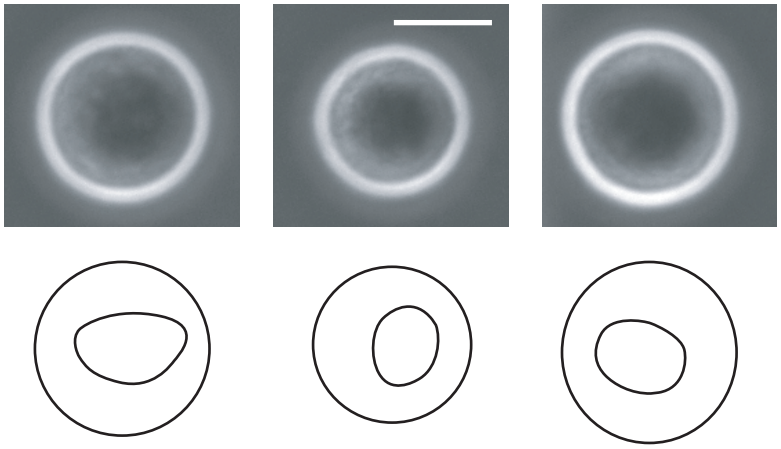

FIG. 6: (Supplemental) Structural anisotropy in suspended CH27 cells arises partially in the form of nuclear asymmetry and off-center location, as shown by phase contrast microscopy (top) and trace of nuclear shape (bottom). Scale bar = 10 μm.

Fluidity as modulated by osmotic challenges to the cell

TABLE II: (Supplemental) Cell size and fluidity as modulated by osmotic challenge (Fig. 7 in the main text). Error is standard deviation. (The distribution of cell size, strictly a lognormally distributed parameter, is sufficiently narrow that the upper and lower standard deviation magnitudes are essentially equal.)

	Condition	Channel blocker	Data set size (cells)	Diameter (μm)	Fluidity
0.7 W/fiber mean laser power:					
Control	Isotonic	None	399	17.7 ± 1.5	0.24 ± 0.09
Hypotonic	1/3 water	None	30	18.0 ± 1.8	0.28 ± 0.09
	1/3 water	NPPB, DCPIB	41	19.7 ± 1.6	0.34 ± 0.14
	1/2 water	DCPIB	20	16.5 ± 1.8	0.22 ± 0.09
	1/2 water	NPPB, DCPIB	19	17.3 ± 2.0	0.27 ± 0.10
	1/2 water	NPPB, DCPIB	25	19.6 ± 1.4	0.41 ± 0.17
Hypertonic	100 mM sucrose	None	25	16.1 ± 1.1	0.23 ± 0.10
	200 mM sucrose	None	20	15.2 ± 1.2	0.20 ± 0.07
	400 mM sucrose	None	22	14.4 ± 1.4	0.14 ± 0.08
1.0 W/fiber mean laser power:					
Control	Isotonic	None	361	17.1 ± 1.9	0.41 ± 0.13
Hypotonic	1/3 water	None	54	18.4 ± 1.8	0.63 ± 0.28
	2/3 water	None	25	17.3 ± 1.7	0.50 ± 0.14
	2/3 water	NPPB	34	18.0 ± 1.6	0.46 ± 0.24
Hypertonic	100 mM sucrose	None	19	14.4 ± 1.0	0.30 ± 0.11
	100 mM sucrose	EIPA	11	13.9 ± 1.1	0.27 ± 0.10
	100 mM sucrose	EIPA	33	15.9 ± 2.0	0.31 ± 0.10
	200 mM sucrose	EIPA	64	15.1 ± 1.8	0.20 ± 0.13
	300 mM sucrose	EIPA	58	14.2 ± 1.6	0.18 ± 0.19

[1] J. M. Maloney, E. Lehnhardt, A. F. Long, and K. J. Van Vliet, "Mechanical fluidity of fully suspended biological cells," *Biophysical Journal*, vol. 105, no. 8, pp. 1767–1777, 2013.